Emergent order in epithelial sheets by interplay of cell divisions and cell fate regulation

Philip Greulich [1,2]

1 School of Mathematical Sciences, University of Southampton, Southampton, UK
2 Institute for Life Sciences, University of Southampton, Southampton, UK

Abstract

The fate choices of stem cells between self-renewal and differentiation are often tightly regulated by paracrine (cell-cell) signalling. Here, we assess how the interplay between cell division, differentiation, and short range paracrine signalling can affect the macroscopic ordering of cell types in self-renewing epithelial sheets, by studying a simple spatial cell fate model with cells being arranged on a 2D lattice. We show in this model that if cells commit to their fate directly upon cell division, macroscopic domains of cells of the same type emerge, if at least a small proportion of divisions are symmetric, except if signalling interactions are laterally inhibiting. In contrast, if cells are first 'licensed' to differentiate, yet retaining the possibility to return to their naive state, macroscopic order only emerges if the signalling strength exceeds a critical threshold: if then the signalling interactions are laterally inducing, macroscopic domains emerge as well. Lateral inhibition, on the other hand, can in that case generate macroscopic patterns of alternating cell types (checkerboard pattern), yet only if the proportion of symmetric divisions is sufficiently low. These results can be understood theoretically by an analogy to phase transitions in spin systems known from statistical physics.

Author summary

A fundamental question in stem cell biology is how a cell's choice to differentiate or not (cell fate choices), is regulated through communication with other cells in a tissue, and whether these choices are a one-way path or to some degree reversible. However, measuring this in living animals is very difficult and often impossible, since this requires to make videos of cells inside the body with a microscope. Here, we employ a simple mathematical model for the fate choices of stem cells when they are regulated by communication with nearby cells in the tissue. We show that different means of cell fate choice and cell communication can lead to qualitatively different patterns of cell types: macroscopic domains, checkerboard patterns, or randomly disordered distributions, depending on the character of cell communication, and whether cell fate is one-way or reversible. Our analysis therefore shows that those aspects of stem cell activity, which are otherwise difficult to measure, can be distinguished by observing macroscopic patterns of cell types.

Introduction

The development of complex tissues requires the appropriate spatial distribution of cell types. In many organs, cell types are ordered in a certain way, either as regular

arrangements, such as hair follicles in skin or crypts and villi in the intestine, or they are clustered into large, yet irregular domains, such as β-cells in Langerhans islets in the human pancreas [1, 2] or prosensory domains in the mammalian inner ear [3]. In other tissues, cell types may be dispersed without apparent order, such as stem cells and committed cells in the basal layers of epidermis [4] and oesophagus [5, 6]. Understanding the emergence of macroscopic order, be it as regular patterns or irregular domains, is one of the fundamental questions of developmental biology.

Historically, pattern formation in biology has also been a fundamental subject of study in mathematical biology. Motivated by Turing's and Wolpert's seminal works on patterning by morphogen signalling [7–9], partial differential equations have often been employed to model the spatiotemporal dynamics of long-range morphogen signalling and cellular responses in a coarse-grained and deterministic manner. However, a cell's choice to acquire a certain cell type identity (*cell fate choice*) is often regulated by paracrine signalling between neighbouring cells, and is also subject to some degree of randomness. An example is the Notch-Delta-Jagged signalling mechanism, which, depending on the relative involvement of signalling pathway factors, can either lead to *lateral inhibition* [10–12], when neighbouring cells mutually repress signaling activity and attain preferably opposite cell type identity, or *lateral induction* [3, 12–15], when neighbouring cells mutually activate signalling and prefer equal cell identity. In this case, stochastic agent models that consider randomness and the system at single-cell resolution, are more appropriate to study the effect of interactions, both at small and large scales.

Understanding the mechanisms underlying the emergence of ordered structures in such systems is of paramount importance for tissue engineering and regenerative medicine. Furthermore, this information may also be used to infer the modes of cell fate choice in tissues, also called *self-renewal strategies* in homeostasis. The most commonly employed method to infer self-renewal strategies is by using clonal data from genetic cell lineage tracing assays [16, 17]. However, competing models can, in homeostatic tissues, often not be distinguished based on clonal data [18, 19]. For example, a long-standing question in stem cell biology is whether cells fully commit to their fate at the point of cell division [4], or whether stem cells fluctuate reversibly between states more or less primed ('licensed' [20]) for differentiation, independently of cell division, before finally committing to terminal differentiation [18, 20, 21]. Only intra-vital live imaging has so far, in few tissues, been able to resolve this question [22–24], yet this technique is difficult and expensive, and not feasible in all tissues. Hence, other ways to distinguish self-renewal strategies by using fixed tissue samples would be invaluable. If it is known how different self-renewal strategies generate qualitatively different macroscopic patterns of cell type distributions, which could be observed using appropriate molecular markers in fixed tissues, such a distinction could be made.

To see whether such an approach could be possible for self-renewing epithelial sheets in homeostasis, we will study a simple model of cell fate choice in a two-dimensional spatial arrangement of cells, and we assess what types of long-range spatial ordering are predicted to emerge for different means of paracrine signalling and self-renewal strategies. In the future, those predictions about qualitative features of cell type patterns can be compared with data representing the spatial distribution of cell-type specific molecular markers, and thereby mechanisms of paracrine signalling and fate choice could be distinguished and inferred.

Models and methods

Model

To analyse order formation in homeostatic epithelial sheets, we model the interplay between divisions of stem cells, cell fate choices, and paracrine signalling between neighbouring cells as a stochastic (Markov) process. We seek to keep this model simple enough to allow theoretical insights and comprehensive understanding, yet sufficiently complete to include the commonly encountered features of signalling, cell fate choice, and lineage hierarchies in homeostatic tissues [4, 18, 25]: we model only two cell types, one which represents self-renewing stem cells at the apex of a lineage hierarchy (cell type A), which can divide long term, while the other one represents cells that are primed ('licensed') or committed to differentiation (cell type B). Furthermore, we assume cells to be spatially arranged in a square lattice formation, which facilitates the analysis of ordering phenomena, as we can compare it with known stochastic lattice models. While in reality, the spatial arrangement of cells in tissues is more complex, the universal nature of critical phenomena such as macroscopic ordering, suggests that these will qualitatively prevail also in more complex arrangements of cells [26]. Finally, cell division and *fate choice* – that is, the process of cells choosing their cell type identity – are modelled by the combination of two standard models [4, 18], expressed schematically as,

$$A \to \begin{cases} A+A \\ A+B \\ B+B \end{cases}, \qquad B \to \emptyset \tag{1}$$

$$A \leftrightarrow B\ . \tag{2}$$

Here, event (1), left, represents the division of A-cells upon which each daughter cell chooses to either remain an A-cell or to become a B-cell, i.e. fate decisions are coupled to cell division [4]. Event (2), on the other hand, allows cell fate choices to occur independently of cell division [18] and instead of committing immediately, B-cells are only 'licensed' to differentiate and retain the potential to return to the stem cell state, A [20]. Finally, event (1), right, represents the extrusion of B-cells from the epithelial sheet (it is assumed that cells continue the differentiation process elsewhere, e.g. in the supra-basal layers of the epithelium, but this is not modelled here). Now, when placing cells in the spatial context, further constraints are introduced. First, we assume that cells can only divide when a neighbouring cell creates space when being extruded from the epithelial sheet. That is, we couple division of an A-cell to the synchronous loss of a neighbouring B-cell, and vice versa. Hence, only where an A-cell is next to a B-cell, written as (A, B), the configuration of cells can change: the B-cell is extruded, $B \to \emptyset$, which is immediately followed by a division of the A-cell, in which one of the daughter cells then occupies the site of the previous B-cell. We can express this as,

$$(A,B) \xrightarrow{\lambda \cdot p_A^\lambda} (A,A), \qquad (A,B) \xrightarrow{\lambda \cdot p_B^\lambda} (B,B)\ , \tag{3}$$

where λ is the rate at which loss, and coupled to it a symmetric division event, is attempted – while this attempt may not be successful if the chosen neighbour is not of opposite cell type. $p^\lambda_{A,B}$ denotes the probability of fate choice A, B, of both daughter cells upon symmetric cell division. Here, we only model symmetric division events of the type $A \to A + A, A \to B + B$ explicitly. While asymmetric divisions, producing an A and a B cell as daughters, are assumed to occur, they do not change the configuration of cells, since this corresponds to the event $(A, B) \to (A, B)$ (we do not consider events $(A, B) \to (B, A)$ as it is commonly observed that stem cells retain their position upon asymmetric division), and are thus not explicitly modelled. Furthermore, cell fate choice

independent of cell division is possible as,

$$A \xrightarrow{\omega \cdot p_B^\omega} B, \qquad B \xrightarrow{\omega \cdot p_A^\omega} A \ , \tag{4}$$

where $p^\omega_{A,B}$ denotes the probability of fate choice A, B, upon an attempted cell fate choice independent of cell division, which happens at rate ω.

Finally, we consider that paracrine (cell-cell) signalling takes place between neighbouring cells, which affects cell fate choice. We model this by allowing the cell fate probabilities $p_{A,B}$ (for simplicity we neglect the superscripts here) to depend on the configuration of neighbouring cell types. In particular, we assume that the fate of a cell on site i depends only on the number of neighbours of type A, $n_A^{(i)}$, and the number of neighbours of type B, $n_B^{(i)}$ (for an update according to (3), this encompasses all six neighbours of the two sites that are updated). Since in homeostasis, the dynamics of the two cell types must be unbiased and thus symmetric with respect to an exchange of all cell types $A \leftrightarrow B$, the cell fate probabilities must be functions of the difference of neighbouring types $n_i := n_A^{(i)} - n_B^{(i)}$. If p_A is increasing with n_i, the excess of neighbouring A cells, this interaction is called *lateral induction*, and if it decreases with n_i, it is called *lateral inhibition* [12]. To select appropriate functions $p_{A,B}$, we first note that the competition between the cell types must be neutral for a homeostatic state to prevail, hence we require that $p_{A,B}(-n_i) = 1 - p_{A,B}(n_i)$, which also implies $p_A(n_i = 0) = p_B(n_i = 0) = 1/2$. Furthermore, the probabilities $p_{A,B}$ should, for very large numbers of neighbours of the same type, tend to $p_A \to 1, p_B \to 0$ (for lateral induction) or $p_A \to 0, p_B \to 1$ (for lateral inhibition) if $n_i \to \infty$ (while the maximum number of neighbours is 4 and 6, respectively, we can in principle extrapolate this function). This asymptotic behaviour suggests a sigmoidal function for $p_{A,B}(n_i)$. We test two types of sigmoidal functions, one representing an exponential approach of the limiting value, modelled as a logistic function, the other one an algebraic approach, modelled as a Hill function. Since $p_A(n_i = 0) = 1/2$, we therefore choose,

$$p_A^{(log)}(n_i) = \frac{1}{2}(1 + \tanh(Jn_i)) \text{ (logistic)} \tag{5}$$

$$p_A^{(hill)}(n_i) = \frac{1}{2}(1 + \frac{Jn_i}{1 + |Jn_i|}) \text{ (Hill)} \ , \tag{6}$$

and $p_B(n_i) = 1 - p_A(n_i) = p_A(-n_i)$. Note that here we used a symmetrized version of a Michaelis-Menten function (Hill function with Hill exponent 1) to assure the symmetry, as other Hill functions cannot be symmetrized in that way.

In the following, we wish to study whether the mode of cell fate choice affects the spatial patterning of cell type distributions. One fundamental question in stem cell biology is whether cell fate is chosen at the point of cell division, or if this choice occurs independently of cell division and is reversible [18, 20]. To address this question, we consider two model versions. In model 1, cell fate is chosen at cell division, i.e. only events (3) occur, whereby the cell fate is then chosen irreversibly according to the probabilities $p^\lambda_{A,B}$ above. In model 2, we assume that cell fate can be chosen independently of cell division, in a reversible manner, i.e. transitions $A \to B, B \to A$ according to (4) can occur, and whether such a switch occurs is then chosen according to $p^\omega_{A,B}$, regulated by signalling from neighbours according to (5) and (6). In the latter version, also cell divisions according to (3) occur, but they are not regulated, so that outcomes (A, A) and (B, B) occur with equal probability. Formally, the two model versions are defined through specific choices of parameter values in the general model, namely,

$$\text{model 1} : \omega = 0 \tag{7}$$

$$\text{model 2} : p^\lambda_A = p^\lambda_B = 1/2 \ . \tag{8}$$

To summarize, we model the system as a continuous time Markov process with cells of type A and B arranged on a square lattice of length L (that is, with $N = L^2$ lattice sites), the possible transitions and parameters as in (3) and (4), together with the functional forms for $p_{A,B}$, (5) and (6), respectively. In particular, we study the model versions 1 and 2, by fixing parameter values according to (7) and (8), respectively.

Methods

To study the stochastic model numerically, we undertake computer simulations following a version of the Gillespie algorithm [27], also called *random sequential update* [28]: during each *Monte Carlo time step (MCS)*, which is a time period defined by the total event rate as $\tau = \frac{1}{\lambda+\omega}$, we choose $N = L^2$ times a lattice site i randomly, with equal probability, and update the chosen site i, as well as a neighbouring site j, when considering an update according to (3). Update outcomes are according to the rules defined in the "Model" section, whereby in general any event that is possible (if the configuration allows it, as in (3)) and occurs with a rate, let's say, γ (e.g. $\gamma = \lambda p_A^\lambda$ in the case of (3), left), is chosen with probability $\frac{\gamma}{\omega+\lambda}$. Through repeated updates, the system evolves. We generally choose a time long enough for the system to settle into a steady state (runtimes of more than L^2 MCS), except for the situations $\omega = 0, J = 0$, when the system is equivalent to the voter model and when mean equilibration times are infinite.

Results

Simulation results

We will now study the two model versions, 1 and 2, numerically and will determine whether long-range order, such as large domains or other patterning, emerges. For convenience, we assign each lattice site i a value $c_i = +1$ if it is occupied by a cell of type A, and we assign $c_i = -1$ if it is occupied by a cell of type B. This allows us to express $n_i = \sum_{j\sim i} c_j$ where $j \sim i$ denotes all sites j neighbouring site i. To assess whether macroscopic domains of cells of equal type emerge, that are of comparable size as the whole epithelial sheet, we measure as an *order parameter* the difference in proportions of A and B cells, $\phi = |\frac{N_A - N_B}{N_A + N_B}|$, where $N_{A,B}$ are the total number of cells of types A, B on the lattice. Hence, $\phi = |\sum_i c_i|$, where the sum is over the whole lattice. The rationale of choosing this measure is that if domains are only small compared to the system size, and we let the system size L be large ($L \to \infty$), then the proportions of A and B cells should become equal in this limit, and $\phi \approx 0$. However, if domains emerge that span a substantial fraction of the whole system, then one or few clusters of one type, A or B, may dominate, leading to a non-zero value of the order parameter, $\phi > 0$. Similarly, we will assess a "staggered" order parameter $\tilde{\phi}$, which measures the emergence of macroscopic patches of a checkerboard pattern, that is, alternating cell types. For that, we generate a 'staggered' lattice with site values $\tilde{c}_i = (-1)^{k_i+l_i} c_i$, where k_i, l_i are row and column index of site i, respectively, and define $\tilde{\phi} = |\sum_i \tilde{c}_i|$. Since the values $\tilde{c}_i$ come from flipping cell types in a checkerboard pattern, any checkerboard pattern in c_i becomes a domain of equal types in $\tilde{c}_i$ and thus $\tilde{\phi}$ measures the emergence of macroscopic patches of checkerboard patterns of cell types.

We simulated the model versions, 1 and 2, for varying values of the interaction strength, J, and the proportion of symmetric divisions, $q = \frac{\lambda}{\lambda+\omega}$, and computed the order parameters ϕ and $\tilde{\phi}$. For model 1, the results are displayed in Fig. 1, both for a logistic cell-cell interaction function $p_{A,B}(n_i)$, according to (5) (left column), and the Hill function, (6) (right column). Notably, both these cases show the same behaviour: the order parameter ϕ is close to zero for any negative value of J, while it raises straight

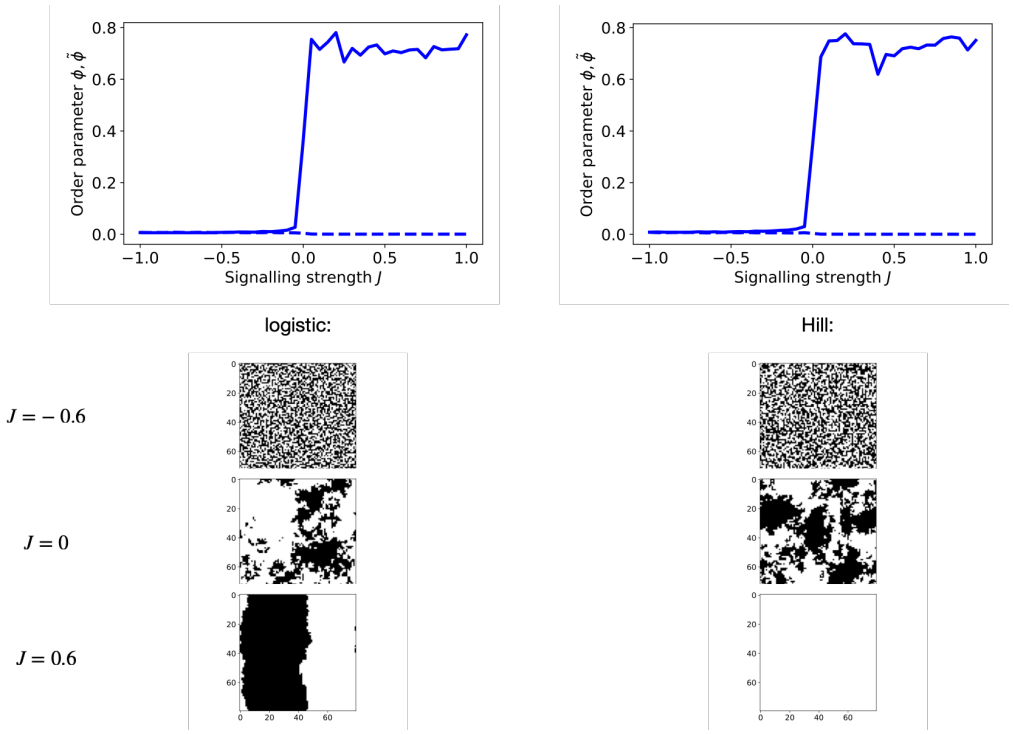

Fig 1. Simulation results for model 1. **Top row:** Order parameters ϕ (bold curve) and $\tilde{\phi}$ (dashed curve) as function of the signalling strength J. The used lattice length is $L = 80$ ($N = L^2 = 6400$ sites) and we simulated for 4000 MCS until computing the order parameters. **Left:** for a logistic interaction function, according to (5), **Right:** for a Hill-type interaction function, according to (6). Below these are the configurations of cell types on the lattice, for logistic interaction function (**left**) and Hill-type interaction function (**right**), for different values of J in each row.

to substantially non-zero values for any $J \geq 0$. $\tilde{\phi}$, on the other hand, is close to zero for any value of J (we have also tested larger ranges, not shown here). Fig. 1 also shows the distribution of cell types on the lattice (bottom), for a negative, positive, and zero value of J, with black pixels representing A-cells and white pixels representing B-cells. As suggested by the order parameters, for negative J no ordering of cells is apparent, one neither sees large domains, nor patterns. For positive J, on the other hand, one sees large domains emerging, even filling the whole lattice. For $J = 0$ we also see large clusters, yet they look qualitatively different to the ones for $J > 0$: The clusters at $J = 0$ have very fuzzy boarders, while those for $J > 0$ have more clearly defined domain borders. Hence, we can conclude that if cell fate is irreversibly chosen at cell division, the default behaviour, for no signalling interaction and for lateral induction, is that macroscopic cell type clusters, in size similar to the system size, emerge. Only lateral inhibition disrupts this order.

For model 2, there are two parameters: J and the proportion $q := \frac{\lambda}{\lambda+\gamma}$ of symmetric cell division events. For $q = 1$ the model is identical to model 1 with $J = 0$, while for $q = 0$ there are no symmetric divisions and cell types switch reversibly with rate ω and probabilities $p_{A,B}$. Fig. 2 shows the order parameters, both ϕ and $\tilde{\phi}$, for $p_{A,B}(n_i)$ being a logistic cell-cell interaction function according to (5) (left column), and a Hill function, according to (6) (right column). In contrast to model 1, we see that for small magnitudes of J, both in negative and positive ranges, both ϕ and $\tilde{\phi}$ are close to zero and thus no long-range ordering emerges. However, at some critical point $J = J_c > 0$

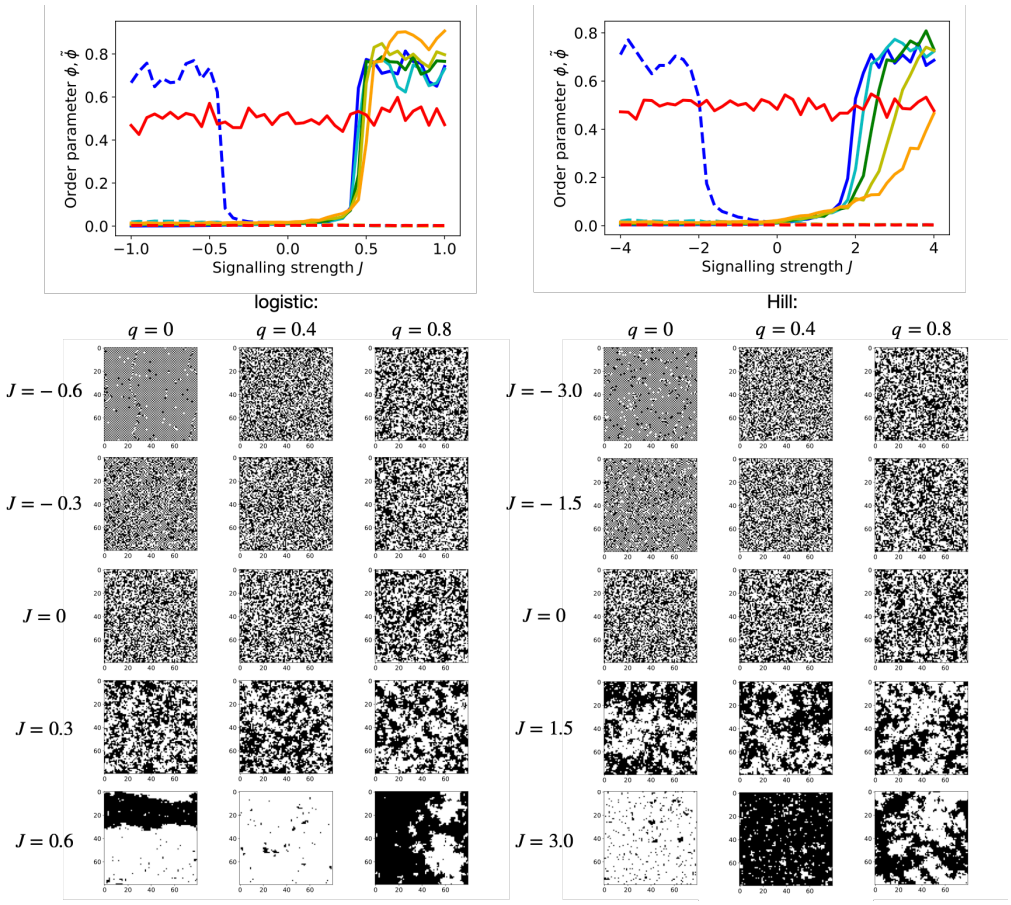

Fig 2. Simulation results for model 2. **Top row:** Order parameters ϕ (bold curves) and $\tilde{\phi}$ (dashed curves) as function of the signalling strength J, for model 2, for different values of $q = \frac{\lambda}{\lambda+\omega}$. The used lattice length is $L = 80$ ($N = L^2 = 6400$ sites) and we simulated for 4000 MCS until computing the order parameters. **Left:** for a logistic interaction function, according to (5), **Right:** for a Hill-type interaction function, according to (6). Below these are the corresponding configurations of cell types shown, for different values of J (rows) and q (columns).

the order parameter ϕ suddenly increases to substantially non-zero values. This feature occurs for both logistic and Hill-type interaction function, although J_c is larger in case of signalling interactions following a Hill function. Furthermore, for $q = 0$ we see a transition in $\tilde{\phi}$ from zero to non-zero values if $J < \tilde{J}_c$ for some $\tilde{J}_c < 0$. We also see this when observing the configurations of cell types on the lattice (bottom of Fig. 2): for sufficiently small values $J < \tilde{J}_c < 0$ and $q = 0$, large checkerboard patterns emerge, while for negative values of J of less magnitude, $\tilde{J}_c < J < 0$, no long-range order is apparent, as is for small positive values $0 < J < J_c$. For large values of $J > J_c$ irregular large-scale domains emerge, for any value of $q > 0$. J_c and $\tilde{J}_c$ differ between the logistic and Hill-type interaction function, but the qualitative features are the same.

We now wish to test whether the observed transitions from $\phi, \tilde{\phi} \approx 0$ to substantial non-zero values are genuine phase transitions, that is, a non-analytic transition from strictly $\phi = 0, \tilde{\phi} = 0$ to non-zero-values at J_c and $\tilde{J}_c$, when $L \to \infty$. Phase transitions are strictly only defined in infinitely large systems, but here we are limited by computational constraints to finite systems. Yet, we can assess this problem by scaling the system size. We show the results in Fig. 3. Here we see that the transitions from $\phi, \tilde{\phi} \approx 0$ to

$\phi, \tilde{\phi} > 0$ become indeed sharper with increasing system size in either model, indicating that $\phi, \tilde{\phi} \to 0$ for $L \to \infty$ in the regime $\tilde{J}_c < J < J_c$, as required for a phase transition. Intriguingly, we see the transition from $\tilde{\phi} = 0$ to $\tilde{\phi} > 0$ in model 2 also for non-zero but small values $q > 0$ (Fig. 3, 3rd row). Furthermore, if we vary q for sufficiently small $J < \tilde{J}_c$, we see that the non-zero regime of $\tilde{\phi}$ prevails also for non-zero values of q as long as $q < q_c$ for some critical threshold value q_c, beyond which it drops sharply to zero (Fig 3, bottom row). Also for this transition, the profile become sharper with system size. This indicates that the ordered phase with macroscopic checkerboard patterns prevails for small, but non-zero proportions of symmetric divisions, q, and only for $q > q_c$ long-range order vanishes. Again this qualitative behaviour is seen for both the logistic and Hill-type interaction function, only the numerical values of q_c vary.

Theoretical insights

To understand the observations made by simulations, we can get insights by mapping the model on a generic two-state spin system as employed in statistical physics. As stated before, we interpret the cell types as numbers $c_i = \pm 1$ which in spin systems can be interpreted as "spin up" ($\uparrow$,+1) and "spin down" ($\downarrow$, -1). We now consider a particular class of spin systems, which we here call *memoryless spin-update models (MSUM)*, as studied in [29], and which are defined by (1) individual sites being randomly chosen, with equal probability, and updated, (2) the probabilities that after the update a spin has value ± 1, called $p_\pm$, may depend on the neighbours of site i, but not on the value of the spin c_i, itself, before the update (hence $p_\mp = 1 - p_\pm$), (3) the spin update probability is symmetric with respect to the neighbour configurations, that is, $p_\pm(-n_i) = 1 - p_\pm(n_i)$. Such systems have been studied and well understood by means of statistical physics [29]. This class of models contains both the voter and the Ising model [30] for particular parameter values. Notably, due to the symmetries of $p_\pm(n_i)$, these functions, and thus the model as a whole, are completely defined by two parameters, namely, $p_1 := p_+(2)$ and $p_2 := p_+(4)$, since due to the symmetry of the function $p_+(n_i)$, all other possible values of p_+ are fixed as $p_+(0) = \frac{1}{2}, p_+(-2) = 1 - p(2), p_+(-4) = 1 - p(4)$, and further $p_- = 1 - p_+$ is fixed (odd values and values outside the range $[-4, 4]$ are not possible, as only the four neighbours of i are considered). In ref. [29] it has been shown that such a system displays a phase transition in the p_1-p_2 parameter plane between an ordered and a disordered phase. This phase transition is of the same universality class as that of the Ising model, except for the particular point $(p_1, p_2) = (3/4, 1)$ at which the system corresponds to the voter model. There, any cluster, which in contrast to the Ising model class have fractal surfaces, diverges over time, so that $\phi \to 1$ for any finite system, yet the mean equilibration time is infinite. A sketch of the phase diagram in the p_1-p_2-plane is shown in Fig. 4, where the dashed black curve sketches the phase transition line.

Now we assess whether our model can be interpreted as a MSUM. First, we consider the rates at which a single site on the lattice is updated according to the model rules (3) and (4). Without loss of generality, let us consider a particular site i on the lattice that contains a B-cell. The rate for this site to change its occupation to an A-cell, either by a change of the cell's identity or by being replaced by an A-cell via the symmetric division of a neighbour, is composed of the rates of two events: (1) the cell type changes according to events (4), with rate ωp_A^ω, or (2) according to events (3) an event $(A, B) \to (A, A)$, occuring with rate λp_A^λ, turns a B cell into an A cell. However, this may occur both if the B cell on site i is selected and if the neighbouring A cell is selected, thus the total rate for this to occur is doubled, $2\lambda p_A^\lambda$. Hence the total rate at which a B cell on site i becomes/is replaced by an A-cell is,

$$\gamma_A(n_i) = \omega p_A^\omega + f_i^A 2\lambda p_A^\lambda = \frac{n_i + 4}{8} 2\lambda p_A^\lambda + \omega p_A^\omega \ , \tag{9}$$

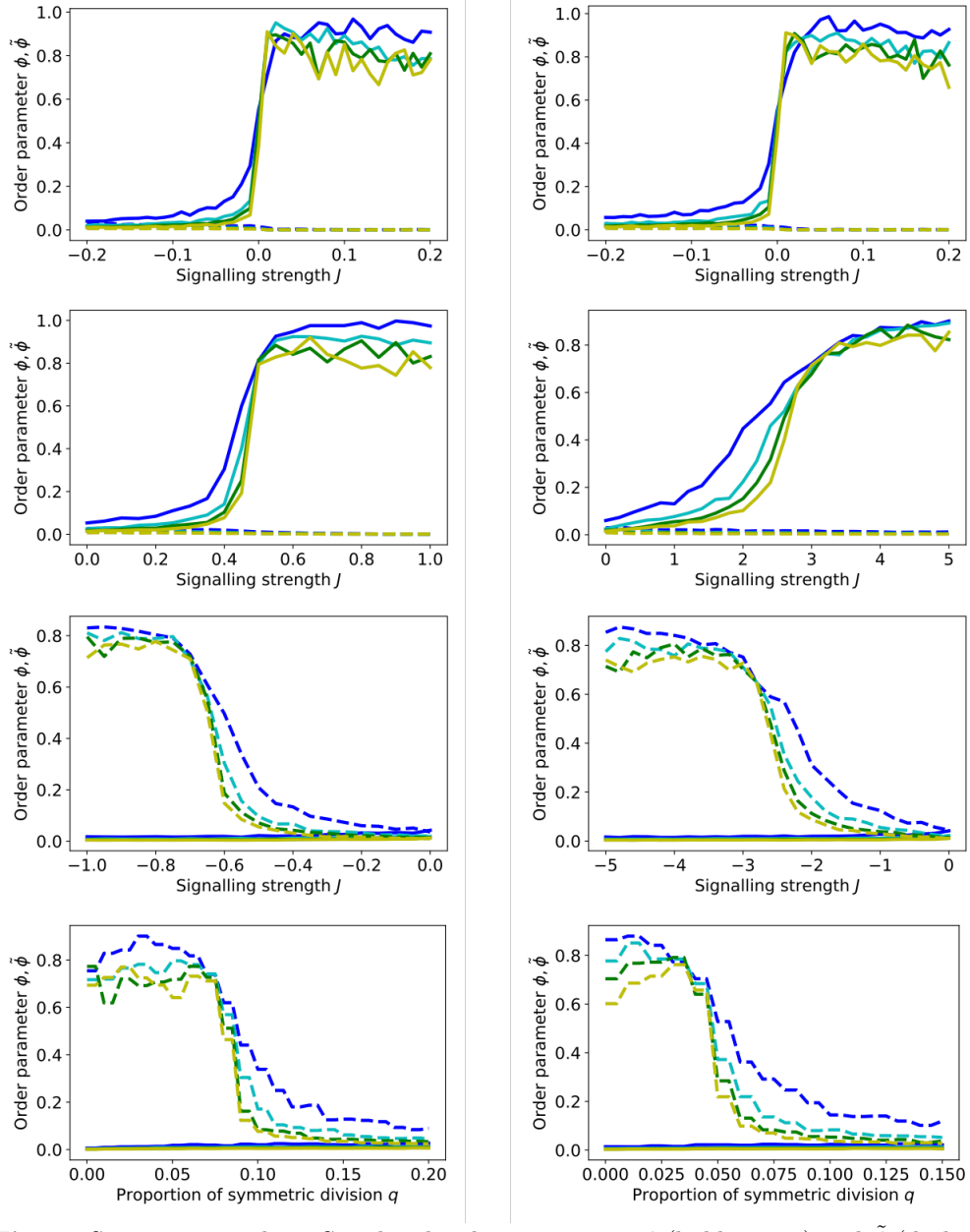

Fig 3. System size scaling. Simulated order parameters ϕ (bold curves) and $\tilde{\phi}$ (dashed curves) as function of J and q, for increasing system sizes $L = 20$ (blue), $L = 40$ (cyan), $L = 60$ (green), $L = 80$ (yellow) and runttimes $L^2/2$ MCS. **Left column:** for logistic interaction function, according to (5). **Right column:** for Hill-type interaction function, according to (6). **Top row:** $\phi(J)$ and $\tilde{\phi}(J)$ for model 1. **2nd row:** $\phi(J)$ and $\tilde{\phi}(J)$ for model 2, with $q = 0.5$. **3rd row:** $\phi(J)$ and $\tilde{\phi}(J)$ for model 2, with $q = 0.05$ (**left**) and $q = 0.02$ (**right**). **Bottom row:** $\phi(q)$ and $\tilde{\phi}(q)$ for $J = -2.0$ (**left**), and $J = -5.0$ (**right**).

where $f_i^A = \frac{n_i+4}{8}$ is the probability that a randomly chosen neighbour of site i is of type A, so that an update according to (3) can occur. For an A cell, the rate to change cell type is analogously $\gamma_B(n_i) = \gamma_A(-n_i) = \frac{-n_i+4}{8} 2\lambda p_B^\lambda + \omega p_B^\omega$.

To see whether this continuous time stochastic process is equivalent to a MSUM, we analyse the random-sequential update scheme (Gillspie algorithm) we used for simulating the system (see "Methods" subsection). We start with model 2, that is, setting $p_A^\lambda = p_B^\lambda = \frac{1}{2}$. If we choose as time unit the update scheme's Monte Carlo time steps $\tau = \frac{1}{\lambda+\omega}$, the probability that a randomly selected site i with a B-cell becomes an A-cell after a Monte Carlo update is $p_{B\to A} = \gamma_A \tau = q\frac{n_i+4}{8} + (1-q)p_A(n_i)$. Similarly, we get the probability for an A-cell to become a B-cell, $p_{A\to B} = \gamma_B \tau = q\frac{-n_i+4}{8} + (1-q)p_B(n_i)$. Crucially, the probability for an A-cell to stay an A-cell is $p_{A\to A} = 1 - p_{A\to B} = q\frac{n_i+4}{8} + (1-q)p_A(n_i) = p_{B\to A}$. Hence, the probability that after the update, site i is occupied with an A-cell is $p_+ := p_{B\to A} = p_{A\to A}$, i.e.,

$$p_+^{(2)}(n_i) = \frac{n_i+4}{8} q + (1-q)p_A(n_i) \ , \tag{10}$$

where $p_+^{(2)}$ is independent of the occupation of i before the update, whether A-, or B-cell (the superscript indicates the model version). The same is valid for $p_- = p_{A\to B} = p_{B\to B} = 1 - p_+$. Furthermore, the function $p_+(n_i)$ is symmetric with respect to the sign of n_i, $p_+(-n_i) = 1 - p_+(n_i)$ and thus model 2 is equivalent to an MSUM with the relevant parameters, according to [29],

$$p_1^{(2)} = p_+^{(2)}(n_i = 2) = \frac{3}{4} q + (1-q)p_A(2) \tag{11}$$

$$p_2^{(2)} = p_+^{(2)}(n_i = 4) = q + (1-q)p_A(4) \ , \tag{12}$$

where p_A can take the two forms of interaction functions according to (5),(6). We further note that $p_A = p_A(n_i, J)$ is also a function of J and thus $p_1 = p_1(J,q)$ and $p_2 = p_2(J,q)$ are functions of both J and q. In Fig. 4, we show trajectories $\boldsymbol{p}(J) = (p_1(J), p_2(J))$ in the p_1-p_2 parameter plane for several values of q (coloured curves), compared to a sketch of the Ising-type phase transition line of MSUMs [29] (black dashed line). We note that those trajectories cross the theoretical Ising phase transition line for values $J_c > 0$, for any $q < 1$. This confirms that model 2 indeed exhibits a phase transition of the Ising universality class at non-zero $J_c > 0$, that is, we see a "ferromagnetic" phase transition from a disordered phase, with order parameter $\phi = 0$ to an ordered phase with $\phi > 0$ that exhibits domains of cell types (i.e. spins) of a size comparable to the system size. The exception is $q = 1$, when the model is identical to the voter model (see discussion of this case below).

We note that switching to the staggered lattice, $c_i \to \tilde{c}_i$, corresponds to replacing $n_i \to -n_i$, since either only c_i flips sign or all its neighbours. For $q = 0$, we have $p_\pm = p_{A,B}$ and since $p_{A,B}$ are functions of Jn_i, $p_\pm$ are symmetric towards the transformation $c_i \to \tilde{c}_i, J \to -J$. Hence, it is expected that $\tilde{\phi} = \phi(\{\tilde{c}_i\})$ exhibits the same phase transition at $\tilde{J}_c = -J_c$ as ϕ does at J_c, yet via emergence of checkerboard patterns instead of domains of equal cell types. This is consistent with the phase transition we observed numerically for $q = 0$ and confirms that $\tilde{J}_c = -J_c$. However, we also observe numerically a phase transition for small non-zero values $q > 0$, in which case the system is not symmetric with respect to $J \to -J, \phi \to \tilde{\phi}$. To understand this, let us consider a situation when $q > 0$ is very small, and $J < \tilde{J}_c$, i.e. when $\tilde{\phi} > 0$. This corresponds to the situation where $J > J_c$ and $\phi > 0$ on the staggered lattice of spins $\tilde{c}_i$, i.e. when the system is within the ordered region of the p_1-p_2 phase diagram (upper right corner in Fig. 4). Any symmetric division within a checkerboard patterned area flips the cell type at one site i, leading to $\tilde{c}_i \to -\tilde{c}_i$. On the staggered lattice, his corresponds either

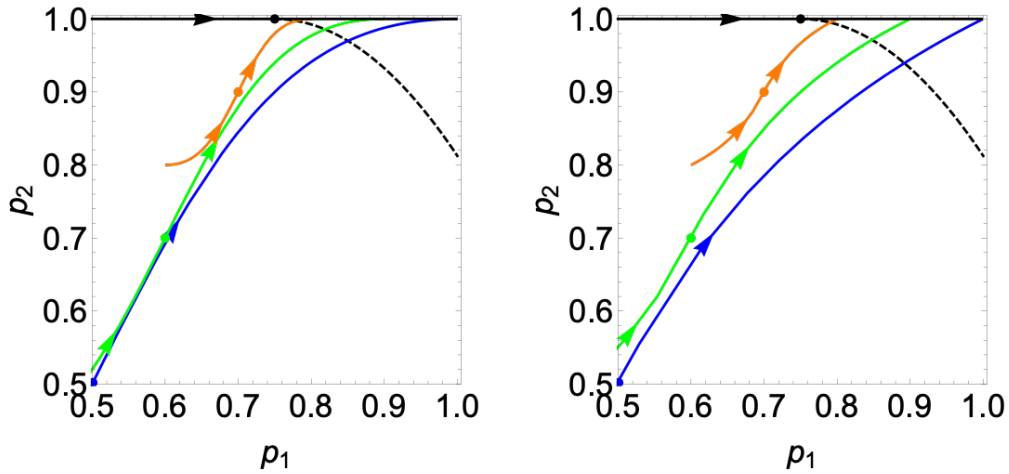

Fig 4. MSUM p_1-p_2 phase space. Depiction of our model's implied MSUM parameters p_1 and p_2 as function of J, $\boldsymbol{p}(J) = (p_1(J), p_2(J))$, within the p_1-p_2 parameter plane, according to (11) and (14) (when substituting (5) and (6), respectively). Displayed are curves for model 1 in steady state (black) and for model 2 and different values of q: $q = 0$ (blue), $q = 0.4$ (green), $q = 0.8$ (red). **Left:** for a logistic interaction function, (5). **Right:** for a Hill-type interaction function, (6). The dots on curves denote the (p_1, p_2) values for $J = 0$, and the arrows show the direction of increasing J. The dashed black line is a sketch of the phase transition line according to [29], which is of the Ising universality class, except for the point $\boldsymbol{p}_v = (0.75, 1)$ which corresponds to the voter model (no exact form for the phase transition curve is available, except for the point $\boldsymbol{p} = \boldsymbol{p}_v$).

to a transition $A \to B$ when $\tilde{n}_i = 4$ or $B \to A$ when $\tilde{n}_i = -4$, meaning that effectively, the probability of symmetric divisions, q, lowers the probability p_4, that is $p_4 \to p_4 - q$. This corresponds to a shift in the parameter plane as $(p_3, p_4) \to (p_3, p_4 - q)$. If q is small enough, the system remains within the regime of the ordered phase (beyond the black line in Fig. 4), while if q becomes larger, it may cross the Ising phase transition line towards the disordered phase.

For model 1, we cannot find a symmetric update probability in general, for any fixed time unit τ. However, if we assume the system to be in the steady state, we can devise an update algorithm that corresponds to an MSUM: as the steady state is time-invariant, we can choose the time unit between updates individually for each update, and do not need to define an absolute time unit. Thus, as before, we undertake a random-sequential update scheme, selecting sites randomly, but use at each update of site i a different time interval between updates, namely $\tau_i = \frac{1}{\gamma_A(n_i)+\gamma_B(n_i)}$. We also simplify the interaction by assuming that the probabilities depend only on the neighbouring cells of chosen site i, and not on those of the other site j involved in a cell division according to (3). Then we get $p_{B\to A} = \frac{\gamma_A(n_i)}{\gamma_A(n_i)+\gamma_B(n_i)} = \frac{(4+n_i)p_A}{(4+n_i)p_A(n_i)+(4-n_i)p_A(-n_i)}$, where we used that $p_B(n_i) = p_A(-n_i)$. Furthermore, $p_{A\to A} := 1 - p_{A\to B} = 1 - \frac{\gamma_B(n_i)}{\gamma_B(n_i)+\gamma_A(n_i)} = p_{B\to A}$, thus the update outcome is independent of the initial value on site i. This means that in the steady state we can define a probability to update to an A-cell, $p_+^{(1)}(n_i)$, being independent of the value on site i, as required for a MSUM:

$$p_+^{(1)} = \frac{(n_i + 4)p_A(n_i)}{(n_i + 4)p_A(n_i) + (4 - n_i)p_A(-n_i)} \,. \tag{13}$$

This update probability is also symmetric, $p_- = 1 - p_+$ and $p_+(-n_i) = 1 - p_+(n_i)$.

Hence, model 1 in the steady state, with the approximation to count only neighbours of the updated site i, constitutes a MSUM. The corresponding relevant parameters are,

$$p_1^{(1)} = p_+^{(1)}(n_i = 2) = \frac{3p_A(2)}{1 + 2p_A(2)} \tag{14}$$

$$p_2^{(1)} = p_+^{(1)}(n_i = 4) = 1 \ . \tag{15}$$

Again, we see the trajectory $\boldsymbol{p}(J)$ plotted in Fig. 4 (black line), which is on the top edge of the diagram, at $p_4 = 1$. Notably, the trajectories for the different interaction functions as given in (5) and (6) both show the same key features: for $J = 0$, we have $p_A(2) = 1/2$ and thus $p_1 = 3/4$, which is exactly the critical point corresponding to the voter model. For any negative J, the system is in the disordered regime, left of the transition line, while for any positive J, it is in the ordered regime, right of the line. Hence, the transition from disordered, with $\phi = 0$, to ordered, $\phi > 0$, occurs exactly at $J = 0$, as we have observed numerically. However, the phase transition is of a different character than the Ising model phase transition. In fact, at the critical point, for $J = 0$, the system is equivalent to the voter model, which does not exhibit a steady state for any infinite system with $L \to \infty$. For any finite system, it will eventually lead to $\phi = 1$, with one species, A or B, occupying every lattice site; however, the expected time for this to occur is infinite.

Discussion

We analysed a model for the cell population dynamics in an epithelial sheet, by modelling cells of two possible types, a stem cell type (A), which can divide, and a cell type primed for differentiation (B), which does not divide, set in a square lattice arrangement. We modelled cell division and differentiation dynamics according to established models of cell fate choice [4, 18, 31], but assumed in addition that fate choices are regulated by paracrine signalling between neighbouring cells. We assessed the the spatial distributions of cell types in the lattice, distinguishing particularly two biologically motivated versions of the model: in one version we assumed that cell fate is chosen and regulated when a cell divides, while in the other version, changes of cell type can occur independently of cell division, in a reversible manner that reflects licensing to differentiate [20]. In either case, we assumed that the propensity of cell fate choice is regulated through signalling which is either "laterally inducing", preferring the choice of the cell type as the majority of neighbouring cells, or "laterally inhibiting", preferring the opposite cell type to that of the majority of neighbours. We modelled this interaction through a probability of fate choice that depends on the number of neighbours of either cell type, through two possible functional forms, a logistic and a Hill-type function. The strength of this interaction is quantified by a single parameter J, whereby positive J corresponds to a laterally inducing interaction, and negative J corresponds to a laterally inhibiting interaction.

Through numerical simulations that we confirmed by theoretical considerations, we found that when cell fate choice is coupled to cell division, the system usually exhibits long-range order, where macroscopic homogeneous domains (cells of equal type) of size similar to the system size emerge whenever there is no regulating interaction or it is laterally inducing. Only for laterally inhibiting interaction, no long-range order is observed. If cell fate is reversible and is regulated independently of cell division, long-range order is generally only observed if the interaction strength $|J|$ exceeds a critical threshold value $J_c > 0$. If signalling is laterally inducing and is sufficiently strong ($J > J_c$), macroscopic homogeneous domains emerge. If the proportion of symmetric divisions is sufficiently low, long-range order emerges also for sufficiently strong inhibiting interactions, if $J < -J_c < 0$, in which case large-scale patterns of alternating cell types,

arranged like a checkerboard, of a size comparable to the system size, emerge. For $|J| < J_c$, no order is observed, that is, all patterns remain small compared to the system size. The observed features are independent of the functional form chosen to model the signalling interaction between cells, both a logistic function and a Hill-type function show the same qualitative behaviour. This means that for modelling such qualitative features, one can choose the type of interaction function freely; preferably such that the analysis is simplified accordingly.

Those findings can be exploited to address some outstanding biological questions. The question whether cell fate is being decided at cell division or independently of it is a long-standing one and has only recently been decided experimentally in few tissues [22–24], through rather complicated and expensive intra-vital imaging assays. Hence, experimental approaches which are feasible and not too expensive are desirable, as the commonly used method of (static) genetic cell lineage tracing combined with clonal modelling turns out to be insufficient to distinguish these cases [18, 19]. A candidate approach to distinguish models of fate choice is by testing them on data about cell type distributions in tissues, which can be obtained by fluorescent microscopy using appropriate cell-type specific markers. While usually the quantitative 'strength' of paracrine signalling interactions cannot be accurately measured, it is often known whether certain signalling pathways are laterally inducing or inhibiting. It has previously been suggested that lateral inhibition can lead to alternating cell type patterns [32, 33] and lateral induction to domains of cells of the same type [3, 15], which also has been shown in some experimental systems (alternating patterns in Drosophila epidermis [34,35] and in *in vitro*-cultured cell sheets [33]; prosensory domains in mammalian inner ear [3]). However, here we showed that further constraints need to be met for such patterns to emerge: if cell fate is reversible, clusters of cell types only emerge if laterally inducing signalling is sufficiently strong, and alternating patterns can only emerge if both the (laterally inhibiting) signalling is sufficiently strong *and* if divisions are predominantly asymmetric, with only a minor contribution of symmetric divisions. From the here-derived additional constraints we can further specify ways to distinguish cell fate choice rules. For example, assume we knew that paracrine signalling is laterally inducing, then the absence of long range ordering suggests that cell fate is reversible, as we have seen that only model 2 may lack order, at least for small interaction strength. On the other hand, the observation of alternating cell type patterns not only implies that the signalling interaction is laterally inhibiting, but also that cell fate choice is reversible, and furthermore, it implies that the proportion of symmetric divisions must be rather small.

Thus, qualitative features of cell type distributions, such as long-range order, express information about the underlying modes of cell fate choice, and by analysing those patterns, conclusions about the reversibility of cell fate, and whether it is decided at cell division or independently of it, can be drawn.

Acknowledgments

The author was supported by an MRC grant MR/R026610/1. The author thanks Ceres Gijsels and Yoshiki Cook for preliminary work related to this article's subject.

References

1. Hoang DT, Matsunari H, Nagaya M, Nagashima H, Millis JM, Witkowski P, et al. A conserved rule for pancreatic islet organization. PLoS ONE. 2014;9(10):1–9. doi:10.1371/journal.pone.0110384.

2. Proshchina AE, Krivova YS, Barabanov VM, Saveliev SV. Pancreatic endocrine cell arrangement during human ontogeny. Acta Histochemica. 2019;121(5):638–645. doi:10.1016/j.acthis.2019.05.010.

3. Hartman BH, Reh TA, Bermingham-McDonogh O. Notch signaling specifies prosensory domains via lateral induction in the developing mammalian inner ear. Proceedings of the National Academy of Sciences of the United States of America. 2010;107(36):15792–15797. doi:10.1073/pnas.1002827107.

4. Clayton E, Doupé DP, Klein AM, Winton DJ, Simons BD, Jones PH. A single type of progenitor cell maintains normal epidermis. Nature. 2007;446:185. doi:10.1038/nature05574.

5. Doupé DP, Alcolea MP, Roshan A, Zhang G, Klein AM, Simons BD, et al. A single progenitor population switches behavior to maintain and repair esophageal epithelium. Science. 2012;337:1091. doi:10.1126/science.1218835.

6. Alcolea MP, Greulich P, Wabik A, Frede J, Simons BD, Jones PH. Differentiation imbalance in single oesophageal progenitor cells causes clonal immortalization and field change. Nature Cell Biology. 2014;16(6):615. doi:10.1038/ncb2963.

7. Turing AM. The Chemical Basis of Morphogenesis. Philosophical Transactions of the Royal Society of London. 1952;237(641):37. doi:10.1400/281797.

8. Wolpert L. Positional information and the spatial pattern of cellular differentiation. Journal of Theoretical Biology. 1969;25(1):1–47. doi:10.1016/S0022-5193(69)80016-0.

9. Green JBA, Sharpe J. Positional information and reaction-diffusion: Two big ideas in developmental biology combine. Development (Cambridge). 2015;142(7):1203–1211. doi:10.1242/dev.114991.

10. Goriely A, Dumont N, Dambly-Chaudiere C, Ghysen A. The determination of sense organs in Drosophila: Effect of the neurogenic mutations in the embryo. Development. 1991;113(4):1395–1404. doi:10.1242/dev.113.4.1395.

11. Collier JR, Monk NAM, Maini PK, Lewis JH. Pattern formation by lateral inhibition with feedback: A mathematical model of delta-notch intercellular signalling. Journal of Theoretical Biology. 1996;183(4):429–446. doi:10.1006/jtbi.1996.0233.

12. Sjöqvist M, Andersson ER. Do as I say, Not(ch) as I do: Lateral control of cell fate. Developmental Biology. 2019;447(1):58–70. doi:10.1016/j.ydbio.2017.09.032.

13. Savill NJ, Sherratt JA. Control of epidermal stem cell clusters by Notch-mediated lateral induction. Developmental Biology. 2003;258(1):141–153. doi:10.1016/S0012-1606(03)00107-6.

14. Boareto M, Jolly MK, Lu M, Onuchic JN, Clementi C, Ben-Jacob E. Jagged-delta asymmetry in Notch signaling can give rise to a sender/receiver hybrid phenotype. Proceedings of the National Academy of Sciences of the United States of America. 2015;112(5):E402–E409. doi:10.1073/pnas.1416287112.

15. Boareto M, Jolly MK, Goldman A, Pietilä M, Mani SA, Sengupta S, et al. Notch-Jagged signalling can give rise to clusters of cells exhibiting a hybrid epithelial/mesenchymal phenotype. Journal of the Royal Society Interface. 2016;13(118). doi:10.1098/rsif.2015.1106.

16. Kretzschmar K, Watt FM. Lineage tracing. Cell. 2012;148:33–45. doi:10.1016/j.cell.2012.01.002.

17. Blanpain C, Simons BD. Unravelling stem cell dynamics by lineage tracing. Nature Reviews Molecular Cell Biology. 2013;14:489–502. doi:10.1038/nrm3625.

18. Greulich P, Simons BD. Dynamic heterogeneity as a strategy of stem cell self-renewal. Proceedings of the National Academy of Sciences. 2016;113(27):7509. doi:10.1073/pnas.1602779113.

19. Parigini C, Greulich P. Universality of clonal dynamics poses fundamental limits to identify stem cell self-renewal strategies. eLife. 2020;9:e56532. doi:10.7554/eLife.56532.

20. Chatzeli L, Simons BD. Tracing the dynamics of stem cell fate. Cold Spring Harbor Perspectives in Biology. 2020;12(6). doi:10.1101/cshperspect.a036202.

21. Krieger T, Simons BD. Dynamic stem cell heterogeneity. Development. 2015;142(8):1396–1406. doi:10.1242/dev.101063.

22. Rompolas P, Mesa KR, Kawaguchi K, Park S, Gonzalez D, Boucher J, et al. Spatiotemporal coordination of stem cell commitment during epidermal homeostasis. Science. 2016;7012(May):1–9. doi:10.1126/science.aaf7012.

23. Ritsma L, Ellenbroek SIJ, Zomer A, Snippert HJ, de Sauvage FJ, Simons BD, et al. Intestinal crypt homeostasis revealed at single-stem-cell level by in vivo live imaging. Nature. 2014;507(7492):362–365. doi:10.1038/nature12972.

24. Nakagawa T, Jörg DJ, Watanabe H, Mizuno S, Han S, Ikeda T, et al. A multistate stem cell dynamics maintains homeostasis in mouse spermatogenesis. Cell Reports. 2021;37(3). doi:10.1016/j.celrep.2021.109875.

25. Greulich P, MacArthur B, Parigini C, Sánchez-García R. Universal principles of lineage architecture and stem cell identity in renewing tissues. Development. 2021;148:dev194399. doi:10.1101/2020.03.10.984898.

26. Ódor G. Universality in nonequilibrium lattice systems: Theoretical foundations. Universality in Nonequilibrium Lattice Systems: Theoretical Foundations. 2008;76(July):1–276. doi:10.1142/6813.

27. Gillespie DT. Exact Stochastic Simulation of Coupled Chemical Reactions. J Phys Chem. 1977;81:2340.

28. Rajewsky N, Santen L, Schadschneider A, Schreckenberg M. The asymmetric exclusion process: Comparison of update procedures. J Stat Phys. 1998;92:151.

29. Drouffe JM, Godrèche C. Phase ordering and persistence in a class of stochastic processes interpolating between the Ising and voter models. Journal of Physics A: Mathematical and General. 1999;32(2):249–261. doi:10.1088/0305-4470/32/2/003.

30. Liggett TM. Interacting Particle Systems. Springer; 1985.

31. Klein AM, Simons BD. Universal patterns of stem cell fate in cycling adult tissues. Development. 2011;138(15):3103. doi:10.1242/dev.060103.

32. Formosa-Jordan P, Ibañes M. Competition in notch signaling with cis enriches cell fate decisions. PLoS ONE. 2014;9(4). doi:10.1371/journal.pone.0095744.

33. Sprinzak D, Lakhanpal A, Lebon L, Santat LA, Fontes ME, Anderson GA, et al. Cis-interactions between Notch and Delta generate mutually exclusive signalling states. Nature. 2010;465:86. doi:10.1038/nature08959.

34. Heitzler P, Simpson P. The choice of cell fate in the epidermis of Drosophila. Cell. 1991;64:1083.

35. De Celis JF, Bray S. Feed-back mechanisms affecting Notch activation at the dorsoventral boundary in the Drosophila wing. Development. 1997;124(17):3241–3251. doi:10.1242/dev.124.17.3241.

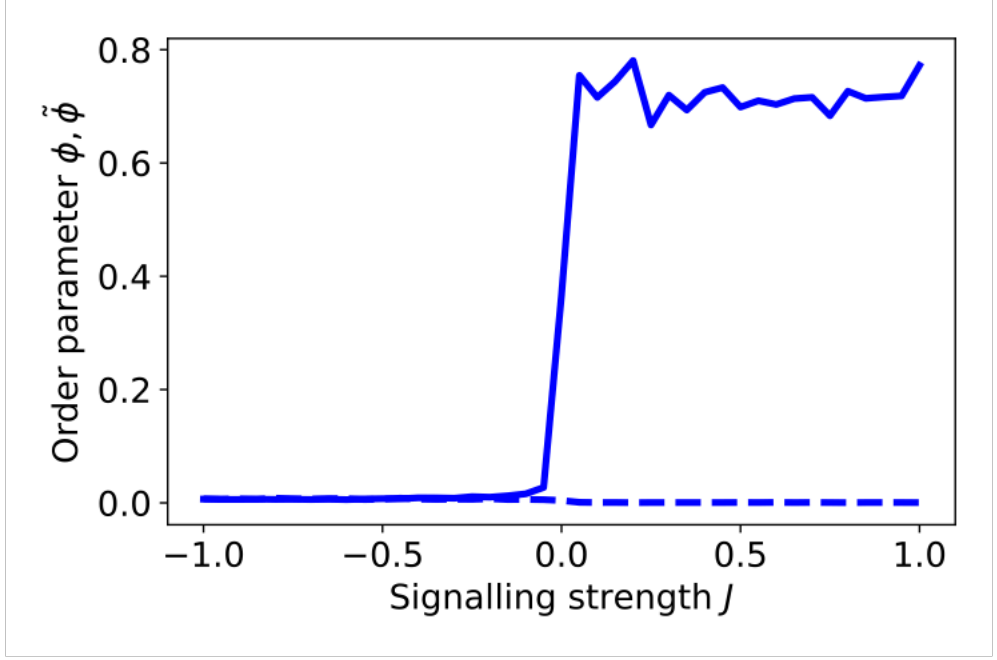

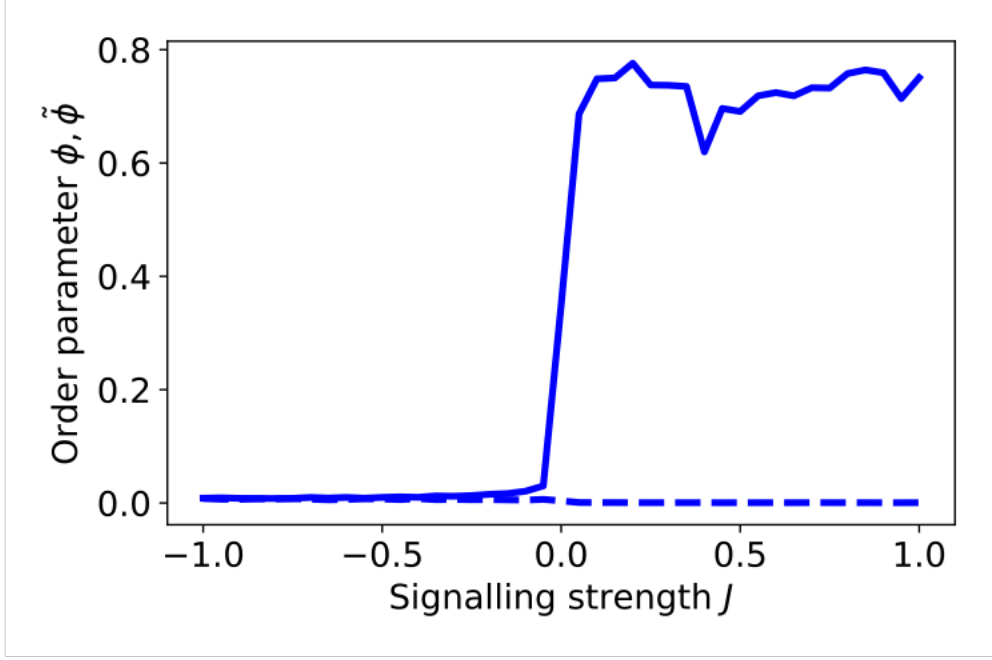

logistic:

Hill:

$J = -0.6$

$J = 0$

$J = 0.6$

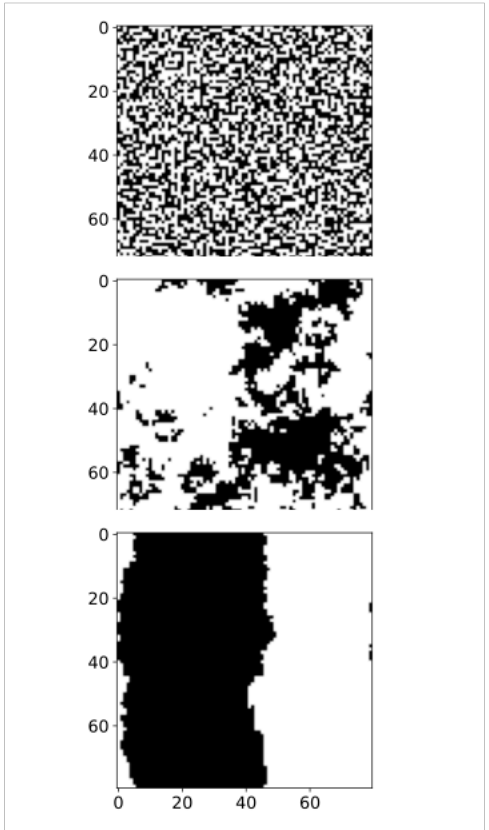

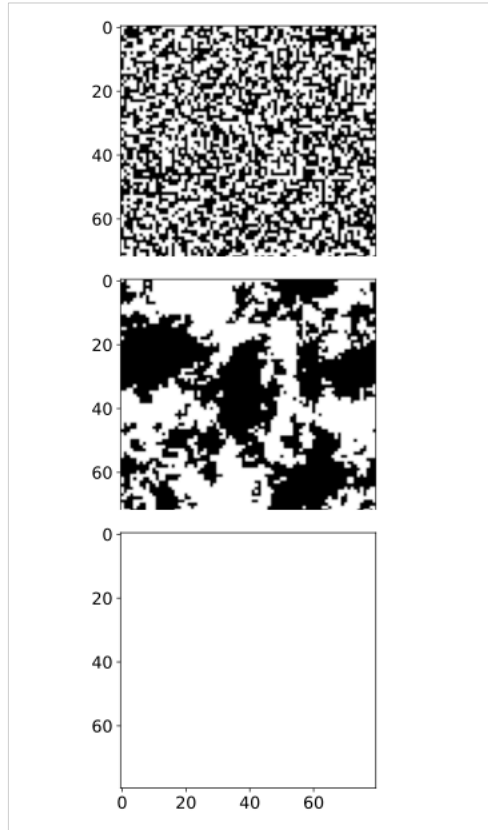

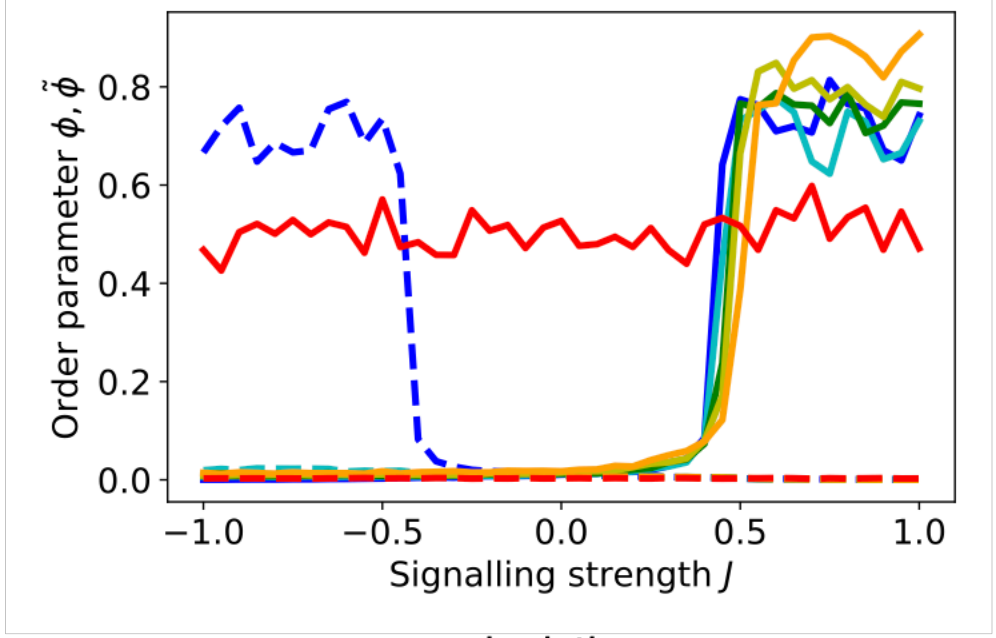

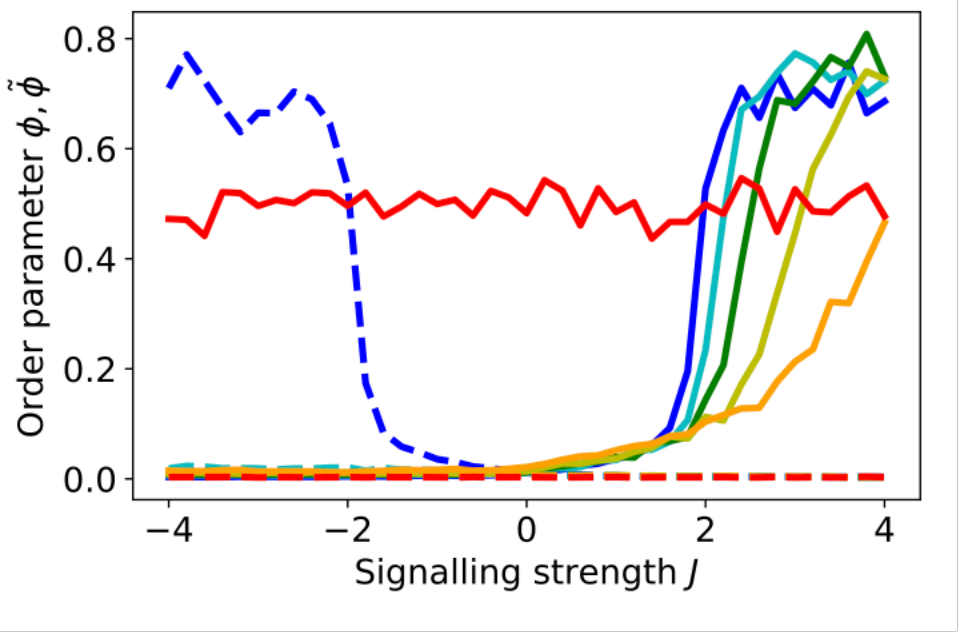

logistic:

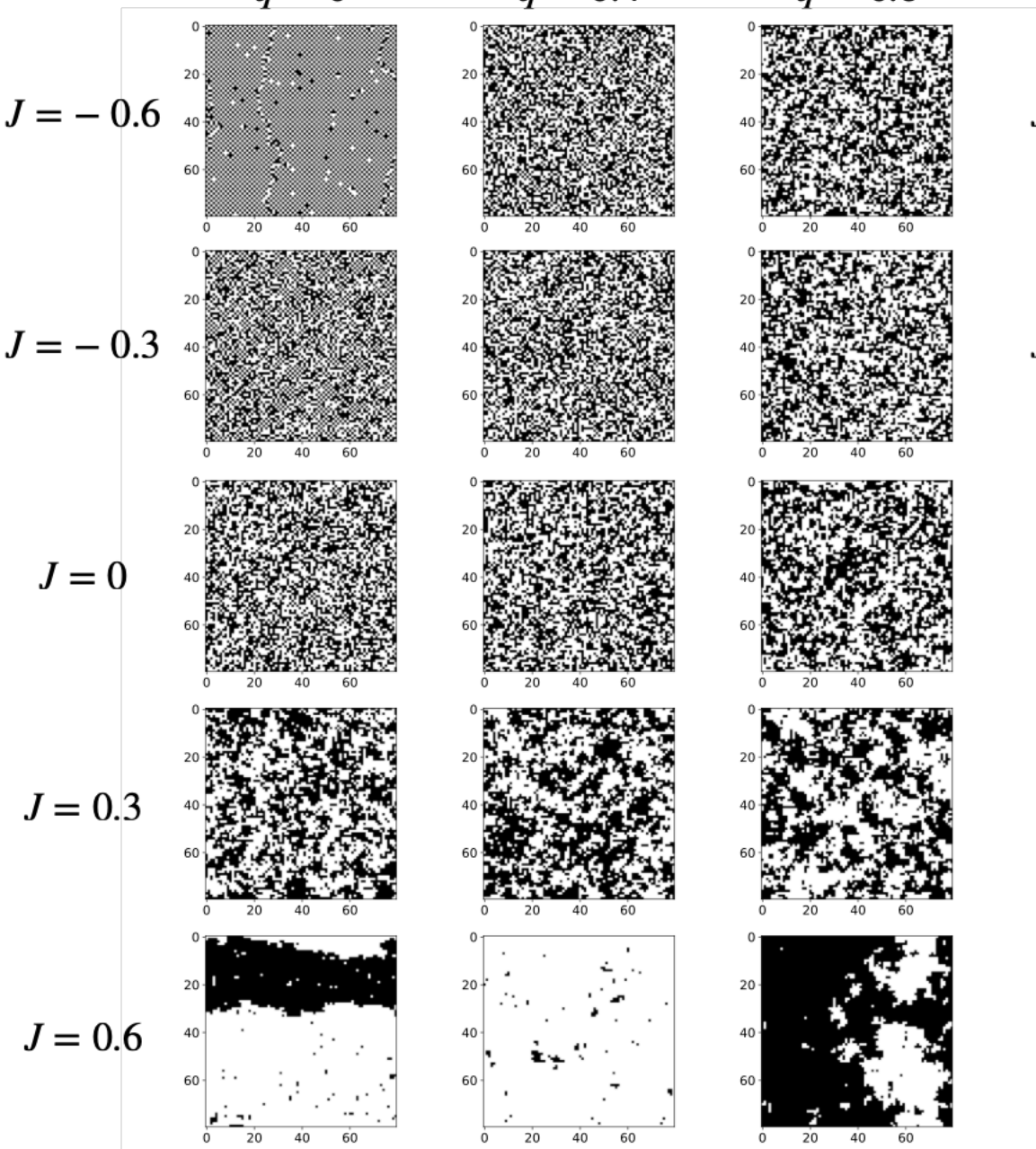

Hill:

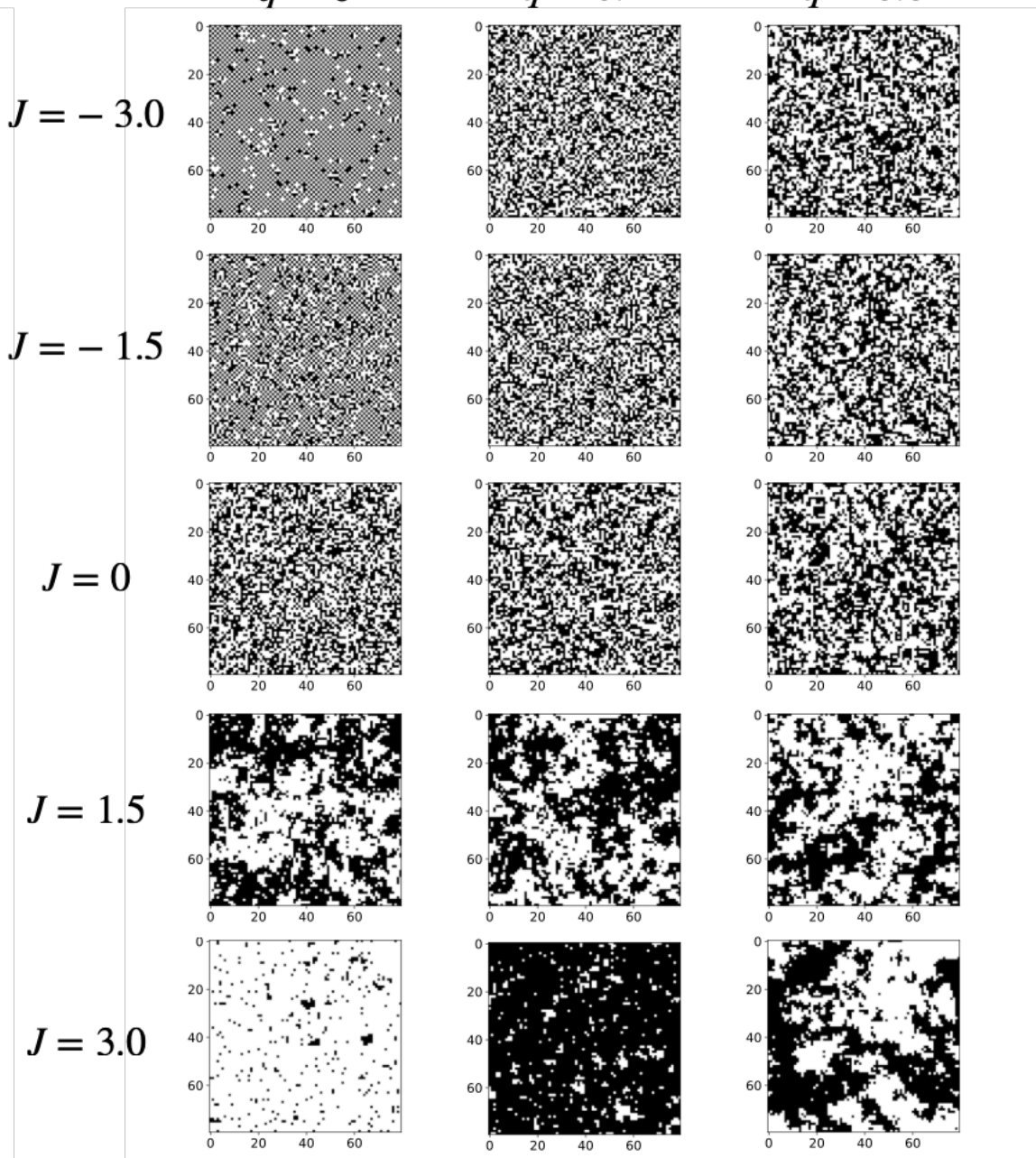

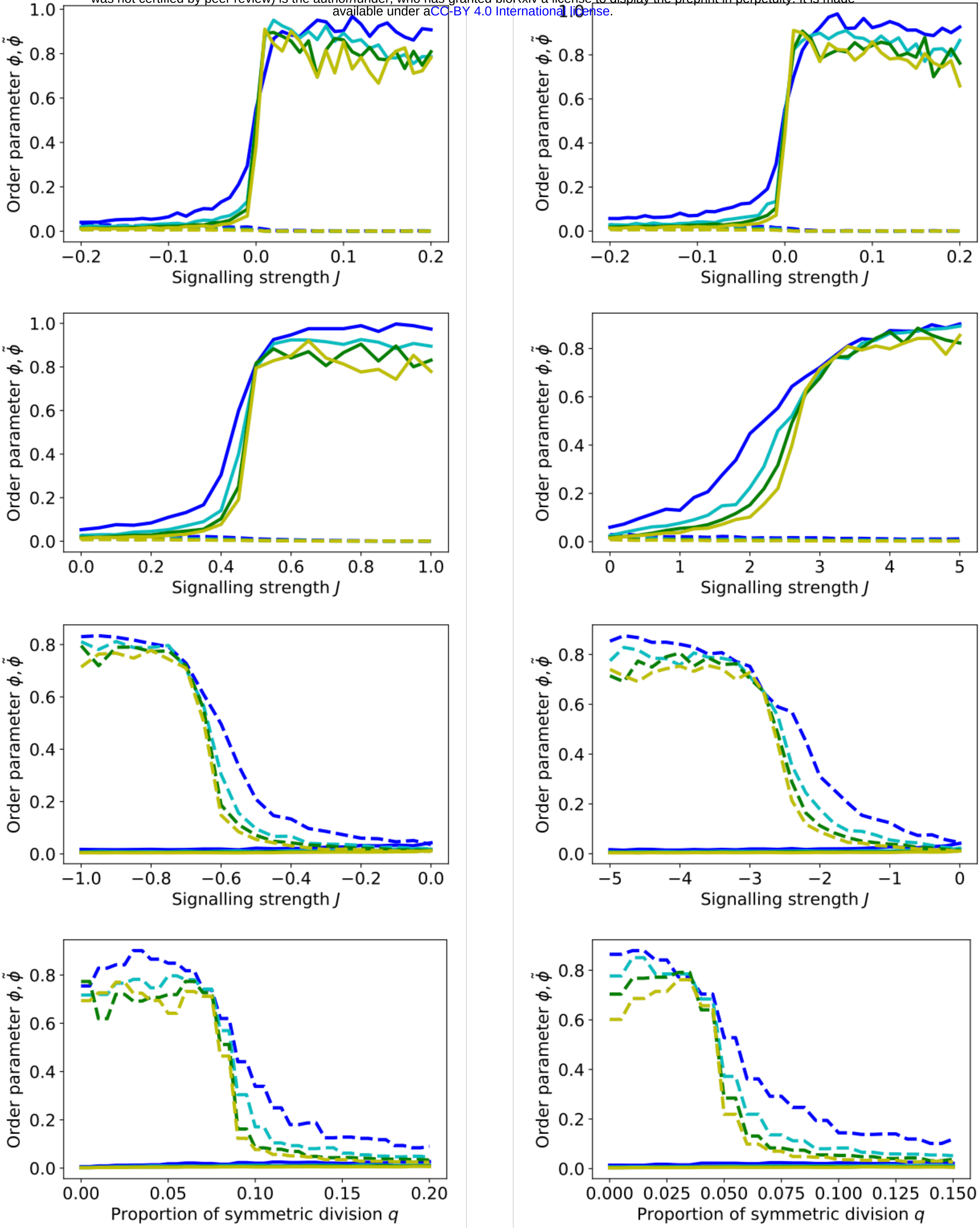

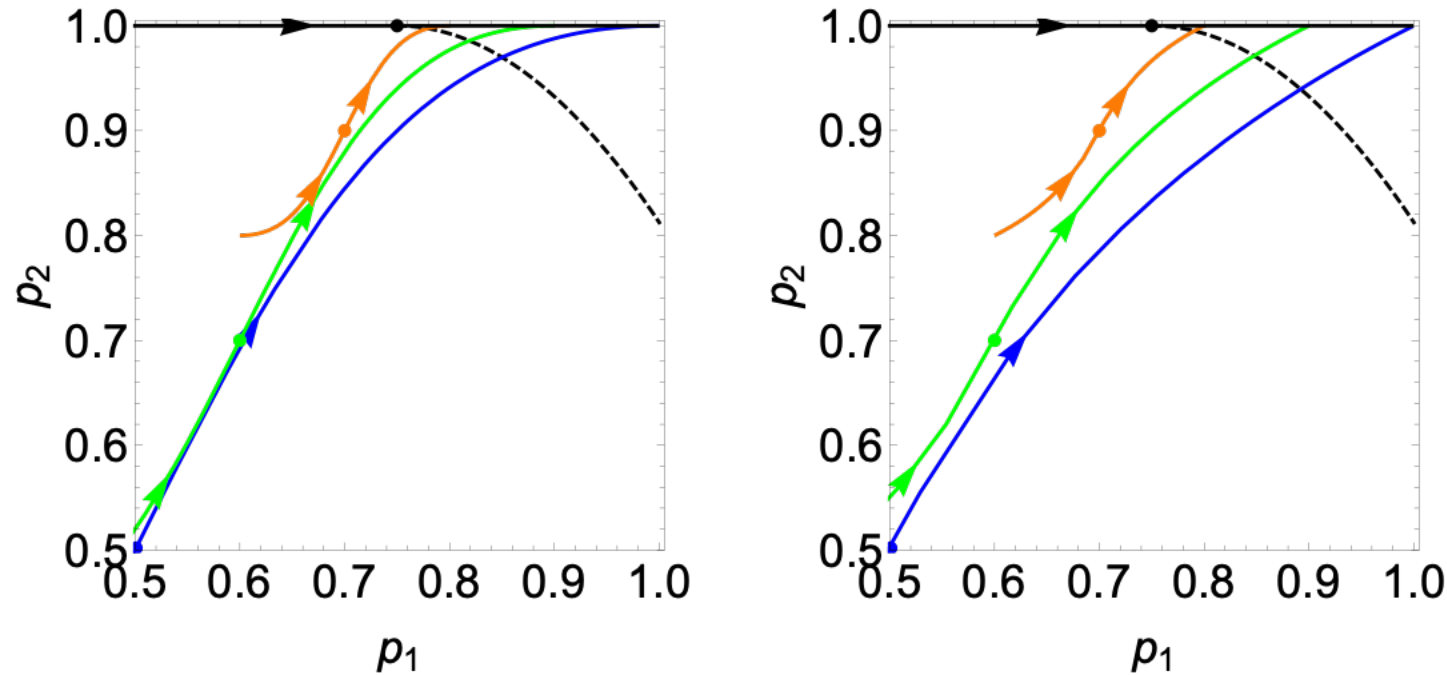
1.0
0.9
0.8
0.7
0.6
0.5
p_2
0.5
0.6
0.7
0.8
0.9
1.0
p_1
1.0
0.9
0.8
0.7
0.6
0.5
p_2
0.5
0.6
0.7
0.8
0.9
1.0
p_1